Electronic Supplementary Information

Facilitating electrocatalytic hydrogen evolution *via* multifunctional tungsten@tungsten disulfide core-shell nanospheres

Liang Ji,[a] Hongyu Cao,[a] Wensi Xing,[a] Shuaicheng Liu,[a] Qian Deng[ab] and Shengping Shen[*ac]

[a] State Key Laboratory for Strength and Vibration of Mechanical Structures, Xi'an Jiaotong University, Xi'an 710049, China.
[b] Department of Engineering Mechanics, School of Aerospace Engineering, Xi'an Jiaotong University, Xi'an 710049, China.
[c] Department of Aeronautics & Astronautics Engineering, School of Aerospace Engineering, Xi'an Jiaotong University, Xi'an 710049, China.
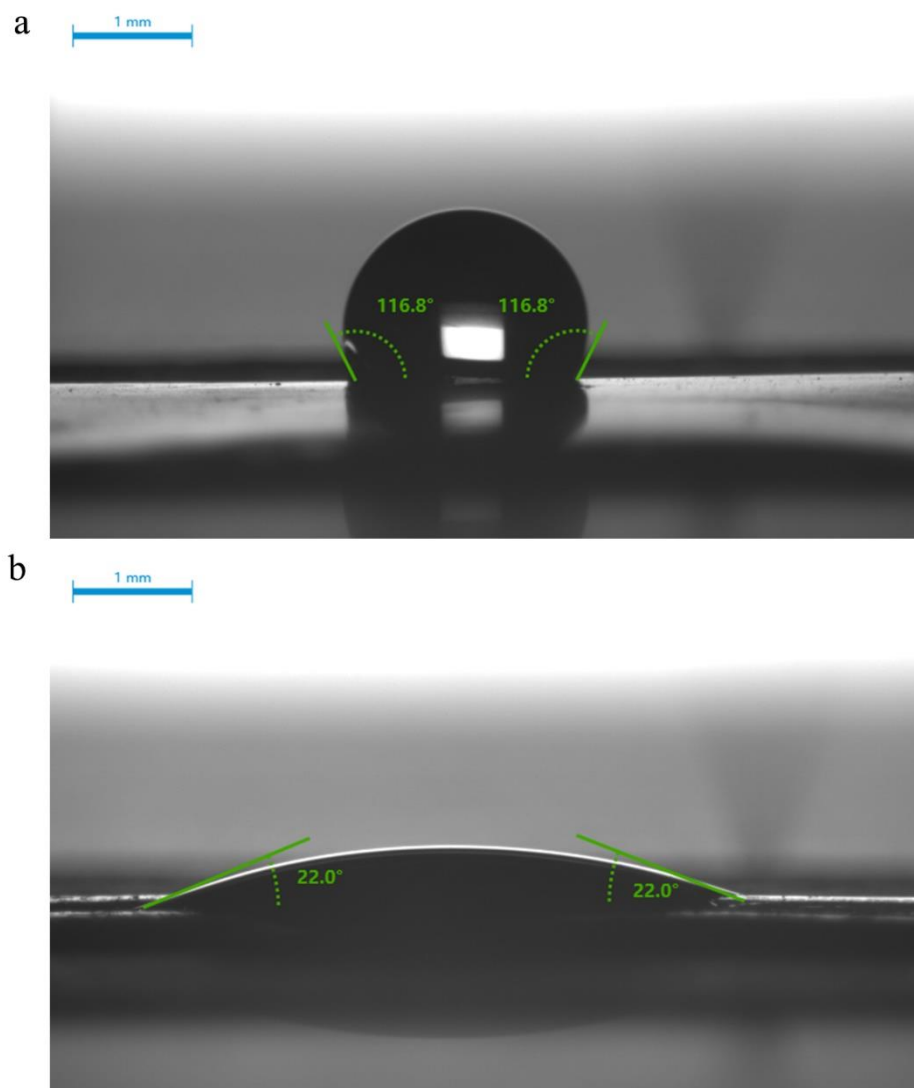[*] Corresponding author. E-mail: sshen@mail.xjtu.edu.cn

This file includes:

Supplementary Figures S1-13

Supplementary Tables S1-2

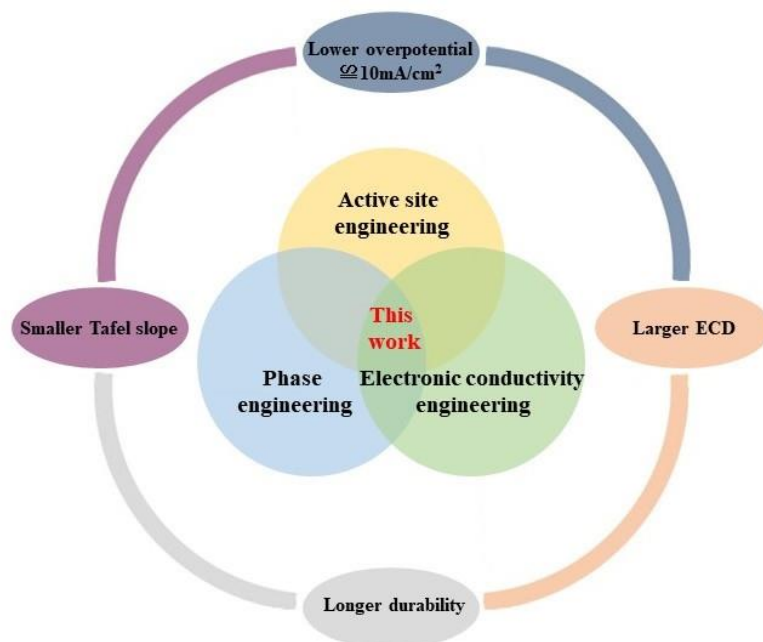Supplementary Equations S1-9

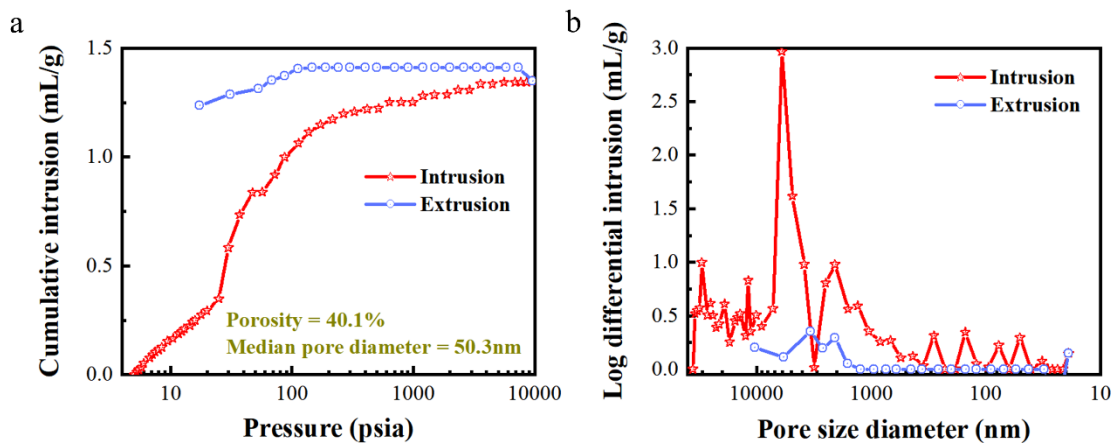Supplementary References
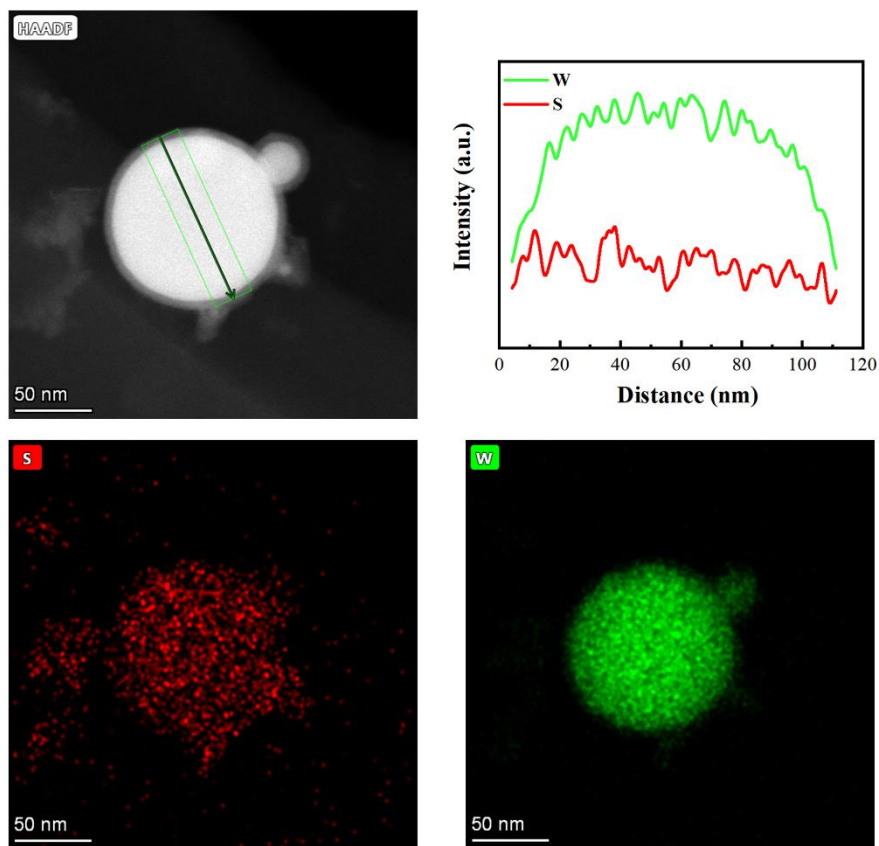
a

1 mm

116.8°   116.8°

b

1 mm

22.0°   22.0°

Fig. S1 Photos of a 2μL 0.5mol H_2SO_4 droplet on (a) MoS_2 and (b) WS_2 surfaces. Water contact angles for MoS_2 and WS_2 are 116.8° and 22.0°, respectively.

**Fig. S2** Aims and strategies of TMDs engineering.

Fig. S3 Mercury intrusion porosimetry tests of the nanoporous electrocatalyst. (a) Intrusion and extrusion curves and (b) pore size distribution.

Fig. S4 EDS mapping of the exfoliated nanosphere. Linear EDS data reveal that the core consists of dense W elements while the shell is made of relatively less dense W-S compounds. EDS signal of W elements is mainly concentrated at the center of CSNS and decreases as the distance away from center increases. Although the nanosphere is ultrathin in TEM tests, it is still a 3D sphere rather than a 2D circle. Therefore, S elements are usually detectable along the chosen line during linear EDS mapping.
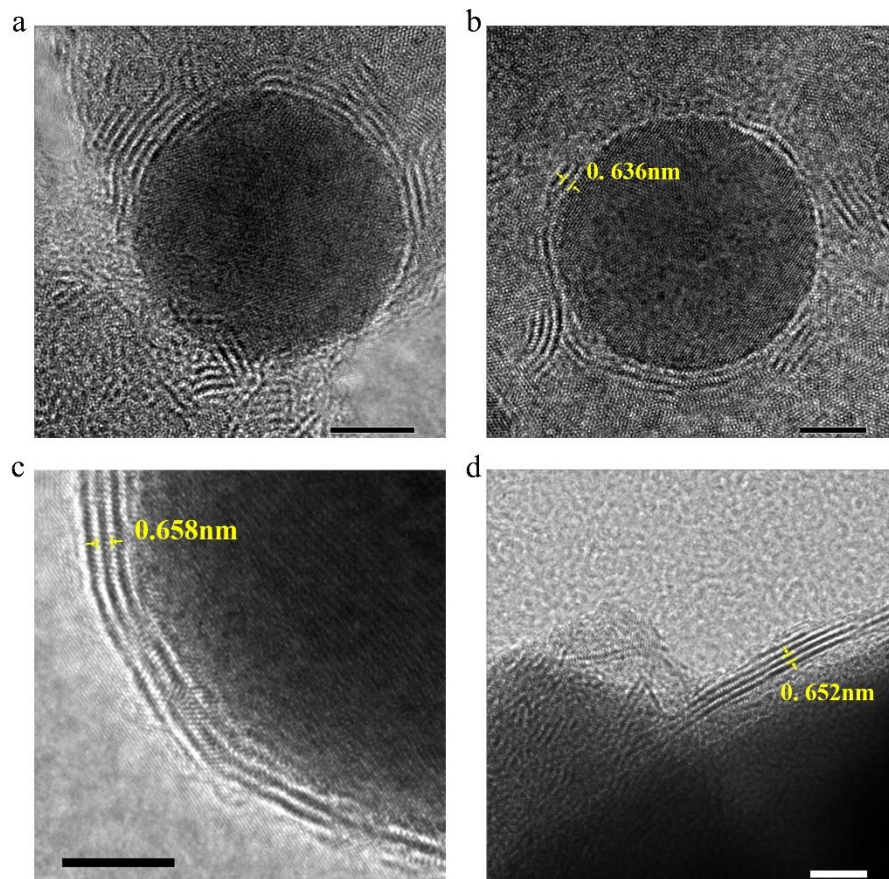
Fig. S5 HRTEM images of the hierarchically curved W-S nanosheets. Scale bars: (a), (b), (c), (d) 5nm.
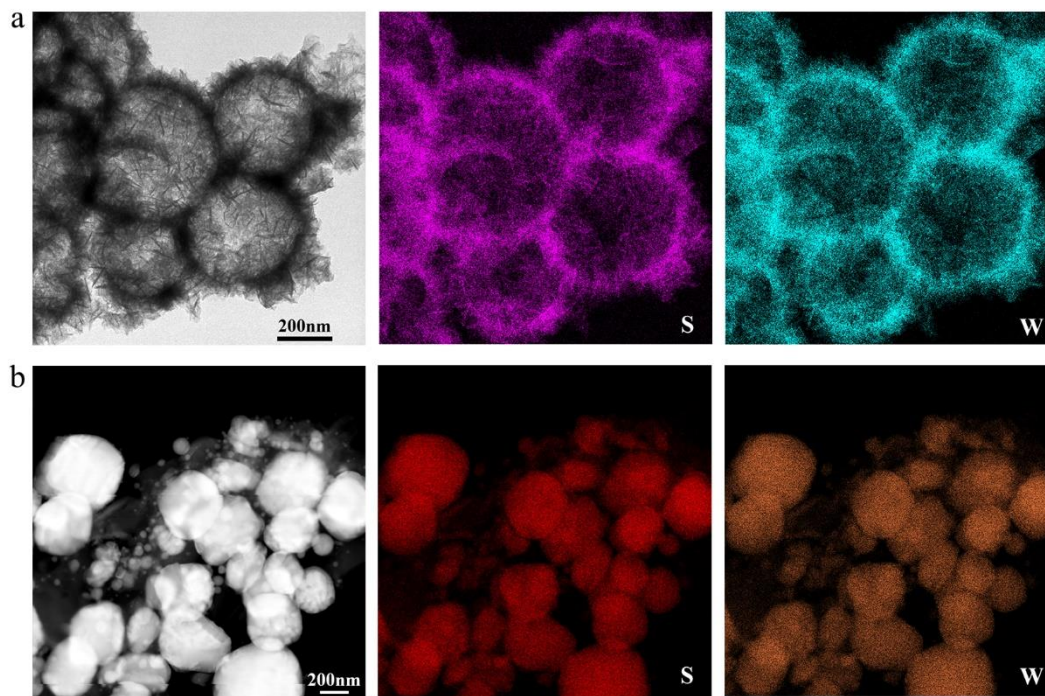
Fig. S6 HRTEM and the corresponding EDS mapping images of (a) WS_2 hollow nanospheres and (b) WS_2 solid nanoparticles.
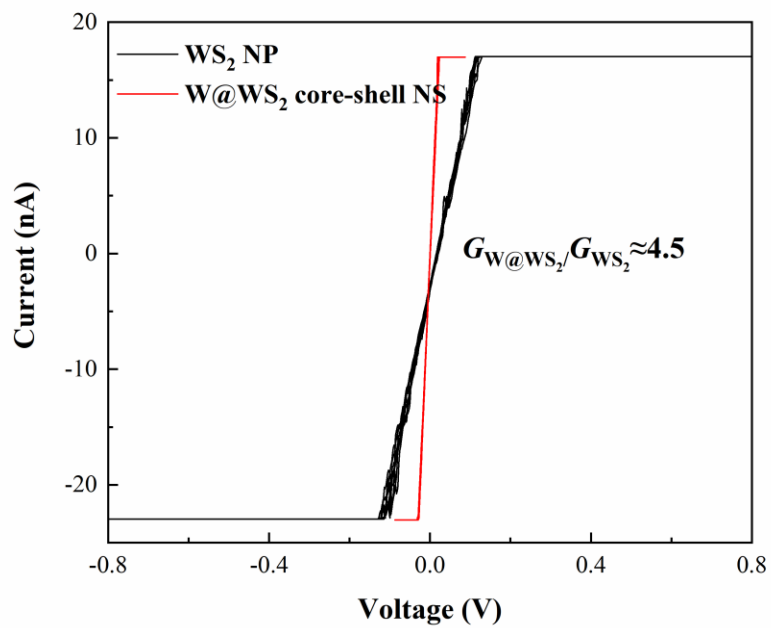
Fig. S7 Electrical conductivities of the WS_2 solid nanoparticles-based electrocatalyst and the W@WS_2 core-shell nanospheres-aggregated electrocatalyst measured by cAFM.
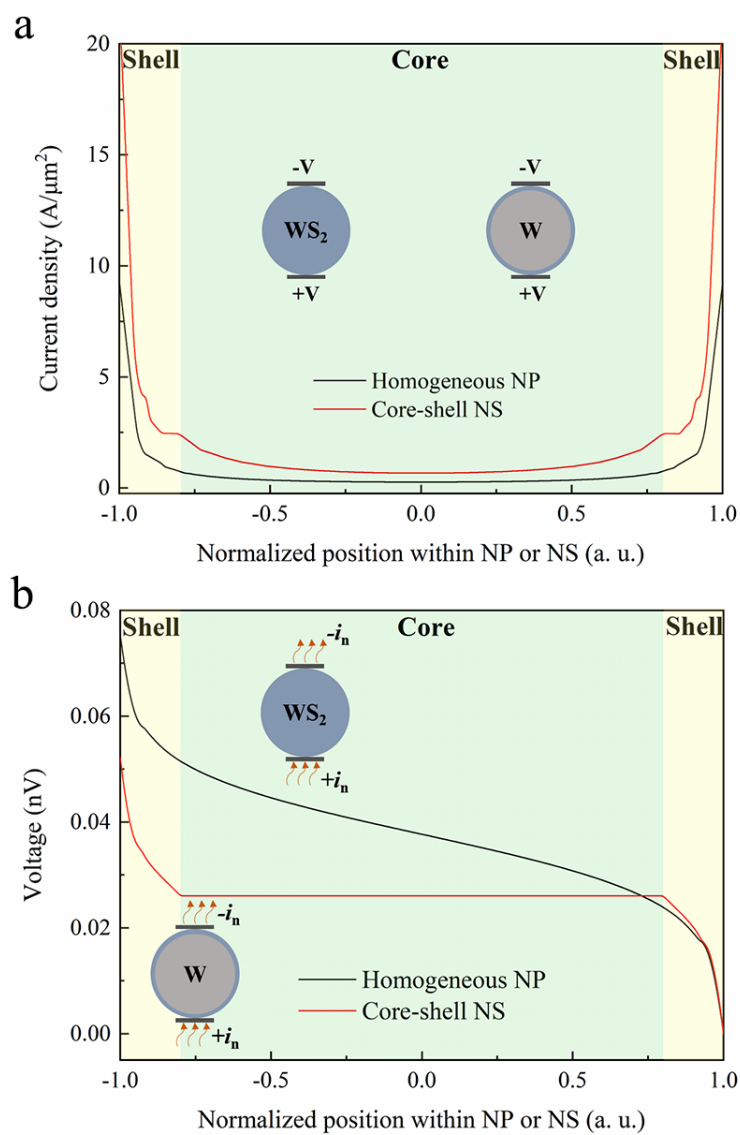
Fig. S8 Electrical property of the WS_2 solid nanoparticle and the $W@WS_2$ core-shell nanosphere under (a) potentiostatic and (b) galvanostatic operations in numerical tests.
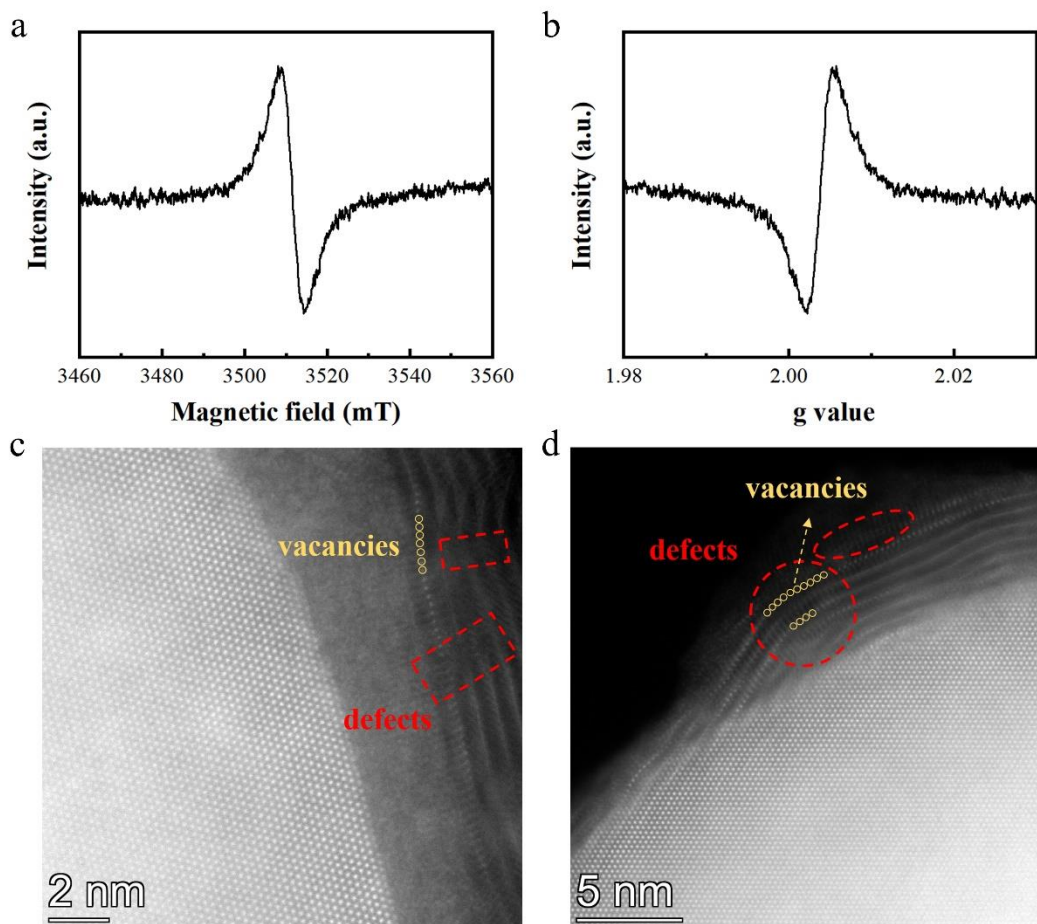
Fig. S9 (a) First order differential spectra of electron paramagnetic resonance of W@WS$_2$ core-shell nanospheres subjected to varying doses. The nature of varying intensity profiles in response to different g values is shown in (b) for demonstrating S-vacancies in samples. (c) and (d), defects on curved WS$_2$ nanosheets characterized by scanning transmission electron microscopy.
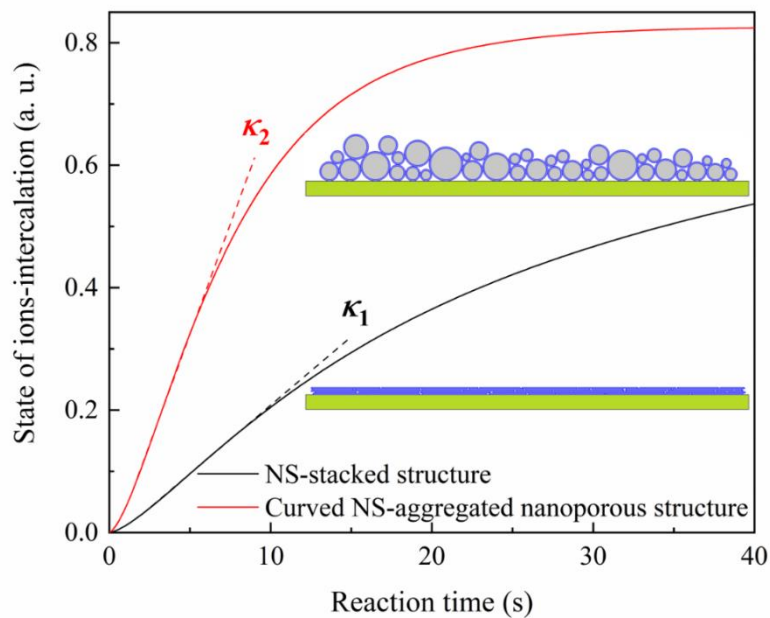
Fig. S10 Comparison between average intercalation rates of the nanosheets (NSs)-stacked structure and the curved NSs-aggregated nanoporous structure. The values of intercalation states 0 and 0.8 represent un-intercalated state and 80% intercalated state, respectively. κ_1 and κ_2 reflect the response rates of NS-stacked and curved NS-aggregated nanoporous structures, respectively. κ_2 is 3.2 times larger than κ_1, which means the response rate is greatly enhanced through core-shell nanospheres.
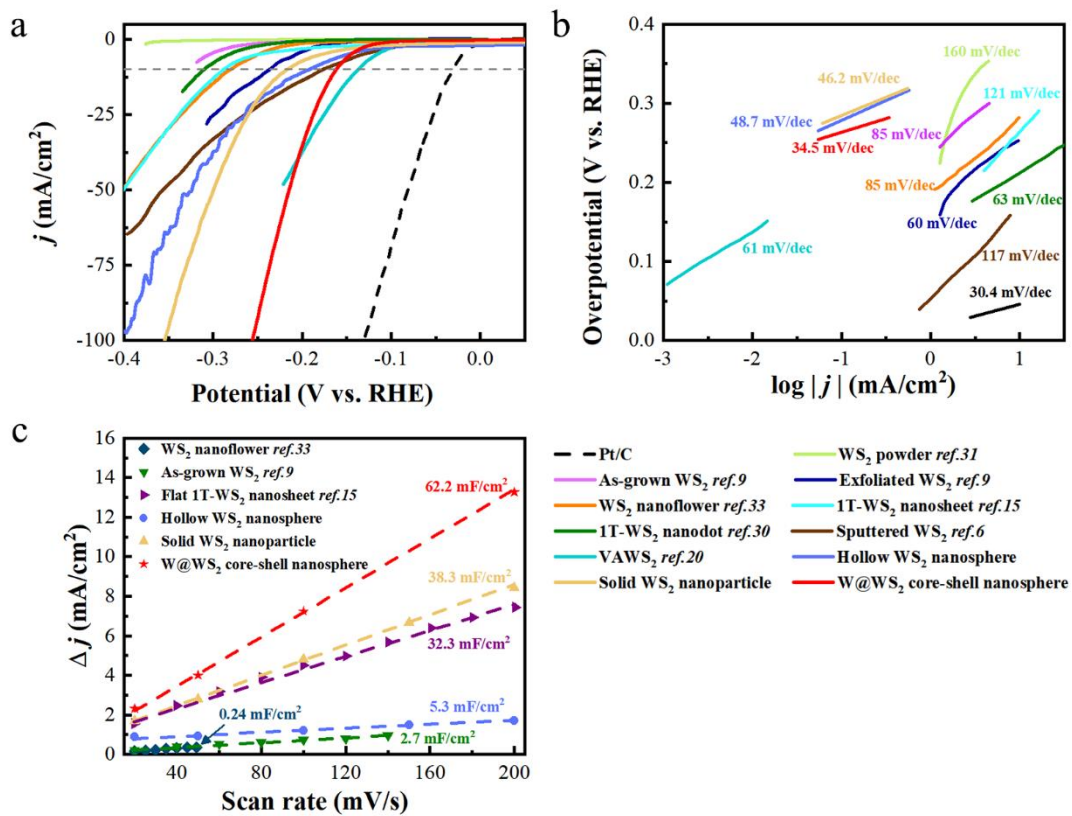
Fig. S11 (a) LSV curves, (b) Tafel plots and (c) capacitive current density versus scan rate of WS$_2$-based electrocatalysts.
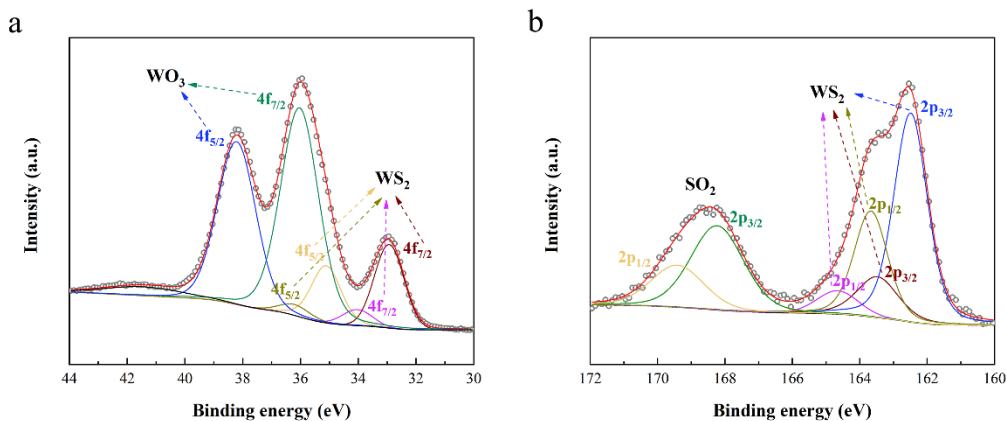
Fig. S12 XPS spectra for (a) W 4f region and (b) S 2p region after durability tests, respectively. After long-term electrochemical tests and storage, WS_2 would react with oxygen to form tungsten trioxide and sulfur dioxide ($2WS_2+7O_2 \rightarrow 2WO_3+2SO_2$). Once the electrocatalyst is put into 0.5mol H_2SO_4 electrolyte, sulfur dioxide would react with water (H_2O) to form sulfurous acid (H_2SO_3). Finally, sulfurous acid would also be oxidized to sulfuric acid (H_2SO_4).
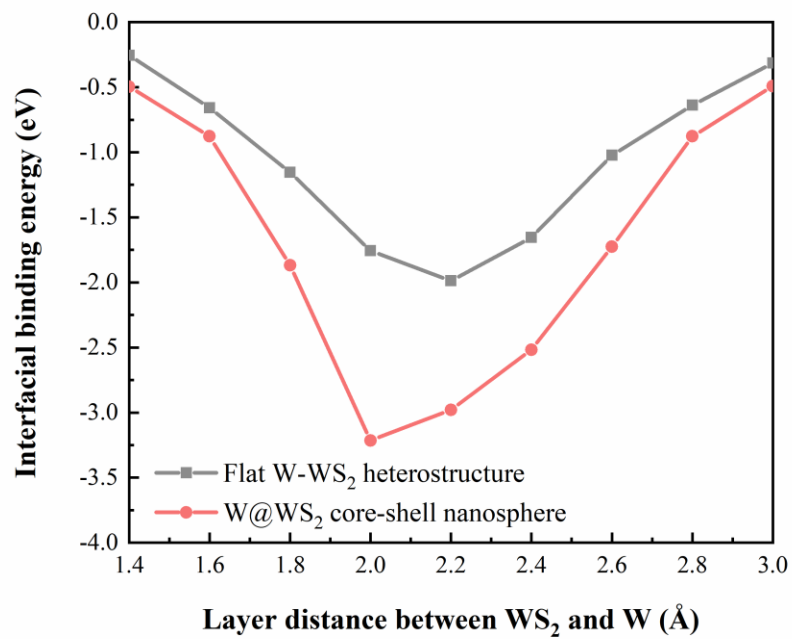
Fig. S13 Interfacial binding energy versus the layer distance between WS_2 and W of flat W-WS_2 heterostructure and W@WS_2 core-shell nanosphere.

Table S1 HER activities of tungsten compounds-based electrocatalysts.

Catalyst	Substrate	Method	Overpotential at 10mA/cm^2 [mV]	Tafel slope [mV/dec]	Durability	C_{dl} [mF/cm^2]	Ref
WS$_2$ powder	GCE	Thermal treatment		160			31
As-grown WS$_2$	Graphite disk	CVD	-330	85		2.7	9
2H-WS$_2$	W foil	SACVT	-137	54	200h	20.3	7
2H-WS$_2$ nanosheets	GCE	Liquid exfoliation	-205	70	500 cycles	24	S1
WS$_2$ film	Carbon cloth	Thermal treatment	-210	68	3h		8
1T-WS$_2$ nanosheets	Carbon cloth	Hydrothermal	-288	121	12h	32.3	15
1T-WS$_2$ nanodots	GCE	Ball milling+Li-insertion	-310	63		8.25	30
WS$_2$ nanoflowers	GCE	Hydrothermal	-280	85		0.12	33
Sputtered WS$_2$	FTO	RF sputter	-178	117			6
VAWS$_2$	W foil	Exfoliation of WO$_3$+low-temperature sulfurization	-140	61	14h		20
WS$_2$ nanoribbons	GCE	Solvothermal	-225	68	1000 cycles		S2
Defect-rich WS$_2$ at 450°C	GCE	Partial sulfurization of WO$_3$	-145	58.5	1000 cycles	31.6	S3
Strained metallic WS$_2$ nanosheets	GCE	Chemically exfoliation	-220	55	120h		S4
20min microwave WS$_2$	W foil	Microwave assisted	-151	70	4h	47.8	9
WS$_2$@HNC NFs	GCE	Coaxial electro-spinning	-282	60	8h		31
WS$_2$/graphene at 350°C	Ni foam	Thermal decomposition	-135	46	8h		12
WS$_2$@P,N, O-graphene	Graphene	Li-insertion+Vaccum filter	-125	52.7	20h		27
WS$_2$/Ni$_5$P$_4$-	GCE	Two-step	-97	74	22h	47.84	13

Ni$_2$P		CVD					
W$_2$C@WS$_2$ NFs	GCE	Hydrothermal	-277	55.4	1000 cycles	12.28	33
MoS$_2$-WS$_2$ heterostructure	FTO	Chemical bath deposition+RF sputter	-129	72	20h		6
ES-WC/W$_2$C	GCE	Calcination	-75	59	480h	97.8	38
Ni(OH)$_2$-WP/CP	Carbon paper	thermal evaporation + electrodeposition	-77	71	18h	28.0	39
Metallic 1T-WS$_2$	GCE	PE-CVD	-347	95	700h		S5
W$_2$C NPs	GCE	carburization	-123	45	10000 cycles		S6
Ni/WC	GCE	Hydrothermal method	-53	43.5	24h	66	S7
W@WS$_2$ core-shell nanospheres	Al foil	One-step pulsed laser-deposition	-161	34.5	~100h	62.2	

Table S2 DFT calculation results.

Nanostructure	Residual stress [Gpa]	Layer distance [Å]	Binding energy [eV]
Flat W-WS$_2$ heterostructure	0.31	2.24	-1.98
W@WS$_2$ core-shell nanosphere	0.17	2.03	-3.21

Formation of WO$_3$ is also beneficial for HER activity and electrical property of the electrocatalyst. Protons and electrons intercalate into WO$_3$ and then H$_x$WO$_3$ is generated:

$$WO_3 + xe^- + xH^+ \rightarrow H_xWO_3 \tag{S1}$$

In this work, mechanism of HER in acids involves two steps. The first is Volmer step, which describes the reaction between a transferred electron and a proton:

$$XS_2 + H^+ + e^- \rightarrow XS_2\text{-}H_{ads} \tag{S2}$$

16

where XS₂ represents TMDs-based electrocatalysts. As a result, an absorbed hydrogen atom is generated on the surface of electrocatalyst. Then, the second step is dominated by Heyrovsky reaction:

$$XS_2\text{-}H_{ads}+H^++e^- \rightarrow H_2+XS_2 \tag{S3}$$
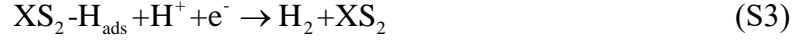
In Heyrovsky step, another electron reacts with the absorbed hydrogen atom and proton to yield H₂.

The rate of HER can be described by Butler-Volmer expression as follows:

$$j = j_0\left[e^{-\frac{nF}{RT}\eta} - e^{\frac{(1-n)F}{RT}\eta} \right] \tag{S4}$$

where n is the number of charge transfer, which equals 2 in Heyrovsky-Volmer mechanism. j_0 is exchange current density, η is overpotential, F is Faraday's constant, R is universal gas constant, T is temperature.

$$j_0 = \frac{RT}{nFAR_{ct}} \tag{S5}$$

where A is geometric area of the electrocatalyst, R_{ct} is charge-transfer resistance, which can be measured in EIS.

The exchange current density can also be expressed as:

$$j_0 = nFkc_{H^+}^{1-n}\left(c_H^{max} - c_H \right)^{1-n} c_H^n \tag{S6}$$

where k is rate constant of HER. With considering n as 2, the exchange current density is:

$$j_0 = 2Fk\left(\frac{c_H}{c_{H^+}} \frac{c_H}{c_H^{max} - c_H} \right) \tag{S7}$$

where c_H and c_{H^+} are, respectively, the hydrogen and proton concentration at the surface of electrocatalyst with the standard state chosen to be the same as used to define the equilibrium potential.

Substituting Equation (S7) into (S4) gives:

$$j = 2Fk\left[\frac{c_H^2}{c_{H^+}\left(c_H^{max} - c_H \right)} \right]\left(e^{-\frac{2F}{RT}\eta} - e^{-\frac{F}{RT}\eta} \right) \tag{S8}$$

The ECSA is calculated from electrical double-layer capacitance (C_{dl}):

$$ECSA = \frac{C_{dl}}{C_s} \tag{S9}$$

where C_s is the specific capacitance of planar sample with smooth surface. For WS_2 tested in 0.5mol H_2SO_4, it approximately equals 60 μF cm^{-2}.[S8]

References

[S1] G. Q. Han, Y. R. Liu, W. H. Hu, B. Dong, X. Li, Y. M. Chai, Y. Q. Liu and C. G. Liu, *Mater. Chem. Phys.*, 2015, **167**, 271-277.

[S2] J. Lin, Z. Peng, G. Wang, D. Zakhidov, E. Larios, M. J. Yacaman and J. M. Tour, *Adv. Energy Mater.*, 2014, **4**, 1301875.

[S3] Y. Ling, Z. Yang, Q. Zhang, Y. Zhang, W. Cai and H. Cheng, *Chem. Commun.*, 2018, **54**, 2631-2634.

[S4] D. Voiry, H. Yamaguchi, J. Li, R. Silva, D. C. B. Alves, T. Fujita, M. Chen, T. Asefa, V. B. Shenoy, G. Eda and M. Chhowalla, *Nat. Mater.*, 2013, **12**, 850-855.

[S5] H. U. Kim, V. Kanade, M. Kim, K. S. Kim, B. S. An, H. Seok, H. Yoo, L. E. Chaney, S. I. Kim, C. W. Yang, G. Y. Yeom, D. Whang, J. H. Lee and T. Kim, *Small*, 2020, **16**, 1905000.

[S6] Q. Gong, Y. Wang, Q. Hu, J. Zhou, R. Feng, P. N. Duchesne, P. Zhang, F. Chen, N. Han, Y. Li, C. Jin, Y. Li and S. T. Lee, *Nat. Commun.*, 2016, **7**, 13216.

[S7] Y. Y. Ma, Z. L. Lang, L. K. Yan, Y. H. Wang, H. Q. Tan, K. Feng, Y. J. Xia, J. Zhong, Y. Liu, Z. H. Kang and Y. G. Li, *Energy Environ. Sci.*, 2018, **11**, 2114-2123.

[S8] W. Liu, J. Benson, C. Dawson, A. Strudwick, A. P. A. Raju, Y. Han, M. Li and P. Papakonstantinou, *Nanoscale*, 2017, **9**, 13515-13526.